JOURNAL OF CATALYSIS 56, 258–267 (1979)

Hydrogenation of Carbon Monoxide over Alkali Metal-Graphite Intercalates. Reaction Selectivity and Catalyst Deactivation Characteristics

MICHAEL P. ROSYNEK[1] AND JOHN B. WINDER

Department of Chemistry, Texas A & M University, College Station, Texas 77843

Received May 19, 1978; accepted September 19, 1978

Alkali metal-graphite intercalates, NaC_{64} and KC_8, and an iron-containing potassium-graphite (4.5 wt% Fe) possess large adsorption capacities for carbon monoxide and exhibit high initial activities for CO hydrogenation at 300°C and 1 atm pressure. Primary hydrocarbon products obtained over sodium-graphite include both paraffins and olefins, while the product distributions over both potassium-based intercalates are limited to saturated hydrocarbons, primarily C_1–C_3, due to the olefin hydrogenation capabilities of these materials. Carbon dioxide generation by a shift reaction is prevented in all cases by the immediate and continuous removal of by-product water via interaction with intercalated alkali metal species. The latter process causes a complete and irreversible loss of catalytic activity after a cumulative conversion that, for KC_8, is equivalent to one CO molecule per three interlamellar potassium atoms/ions, suggesting a lack of interlayer penetration by CO rectant. In the case of iron-containing potassium-graphite, no residual hydrogenation activity ascribable to the transition metal component remained following total destruction of intercalated potassium. Adsorption and subsequent reaction of carbon monoxide over all of these materials apparently occurs on sites associated with intercalated alkali metal species located primarily along the exposed edges of graphitic planes.

INTRODUCTION

Crystalline graphite forms a wide variety of stable intercalation compounds with such species as alkali metals, halogens, metal halides, and others (*1–5*). In many of these substances, the atoms, molecules, or ions of the intercalated species are not merely distributed randomly between the layers of the graphite structure, but have an ordered layer-lattice of their own, and the corresponding interlamellar compounds often exhibit well-defined stoichiometric compositions. Alkali metal-graphites, for example, can exist in at least five distinct "stages" of composition, viz., XC_8, XC_{24}, XC_{36}, XC_{48}, and XC_{60} (where X = K, Rb, or Cs), which differ from each other in both the internal structure of each alkali metal layer and in the repeat frequency of such layers with those of the graphite structure itself (*6*). The saturated, first-stage compounds (XC_8) contain hexagonally ordered planes of alkali metal atoms that alternate with each carbon layer and cause a swelling of the graphite lattice. In the case of KC_8, for example, the graphitic interlayer distance is increased from the normal 3.35 to 5.41 Å (*7*). The saturated stage of sodium-graphite, nominally NaC_{64}, on the other hand, is considerably less well defined, both structurally and stoichiometrically, than those of the heavier alkali metals.

[1] To whom all correspondence should be addressed.

0021-9517/79/020258-10$02.00/0

Characteristic of these and related compounds is a partial or complete ionization of the inserted species and a consequent transfer of electron density to or from the π-system of the graphite lattice, the direction of transfer depending on the electron doning or accepting tendencies of the intercalated entities (*8*). Such a charge–transfer process alters the electronic and magnetic properties of both the guest and host species and, in certain cases, imparts to the resulting donor–acceptor complex both a "transition metal-like" electronic nature and a corresponding catalytic behavior that are typical of neither of its separate components. The extents of ionization of graphite-inserted species vary widely, being almost negligible in the case of halogen-graphites, and as high as 30 to 40% for first-stage potassium-, rubidium-, and cesium-graphites (*9*).

Although such inclusion compounds of graphite have been known for at least 50 years, their unusual catalytic and surface properties, particularly those of the alkali metal-graphites and their derivatives, have only recently begun to be explored (*10*). Alkali metal-graphites, both in pure form and in the presence of reduced or partially reduced cointercalated transition metal chlorides, have been reported to possess varying degrees of catalytic activity for several reactions of the "hydrogen-activating" type, including hydrogenations of carbon monoxide (*11*, *12*), carbon dioxide (*13*, *14*), olefins (*15*), and aromatics (*16*), double-bond isomerizations of olefins (*17*), and the synthesis/decomposition of ammonia (*18*, *19*). Despite these studies, however, many details of the catalytic properties of these materials for certain reactions remain obscure and their behaviors ill-defined. We have qualitatively examined in more detail the catalytic behaviors of sodium- and potassium-graphite intercalates and of an iron-containing potassium-graphite for the hydrogenation of carbon monoxide, with particular emphasis on establishing reaction selectivities and catalyst deactivation characteristics.

EXPERIMENTAL METHODS

Materials. Hydrogen (99.995%) and carbon monoxide (99.97%) reactants were Linde research grade and were passed through a trap at −196°C before use. Metallic sodium and potassium, each having a purity of 99.95 mole%, were obtained in vacuum-sealed ampoules from Callery Chemical Co., and were used without further purification. Powdered graphite (200/250 mesh) was Union Carbide Co. No. SP-1 spectroscopic grade, with a total ash content of <1 ppm and a measured BET-N_2 surface area of 2.0 m^2/g. The iron/alumina comparison catalyst was Harshaw Chemical Co. No. FE-0301, and was supplied as 20 wt% of Fe_2O_3 impregnated on 0.32-cm tablets of activated alumina. The latter were crushed and sized to 40/80 mesh granules, evacuated for 16 hr at 400°C, and treated with an excess of circulating H_2 for 8 hr at the latter temperature, with continuous removal of reduction products by an in-line trap maintained at −196°C, followed by overnight evacuation at 300°C to a residual pressure of $<10^{-5}$ Torr. The reduced catalyst had a measured BET-N_2 surface area of 42 m^2/g, and 0.47-g (reduced weight) samples were used for all experiments in which this material was employed.

Apparatus. All hydrogenation experiments were performed in the gas phase using a stirred-batch reaction system of the closed-loop, recirculation type. The system consisted of an all-glass circulation pump, a U-shaped Pyrex reactor with spiral preheater section, and a micro-volume gas sampling valve with evacuable sample loop for periodically removing 0.3 vol% samples by expansion for gas chromatographic analyses. Total system volume was 340 ml, 85% of which was contained in a spherical mixing vessel located just upstream of the reactor. The reaction system was connected

TABLE 1

Average Initial Rates of CO Hydrogenation over Graphite Intercalates and Iron/Alumina at 300°C and an Initial H_2/CO Reactant Ratio of 4/1[a]

Catalyst	Average initial reaction rate (moles of CO/sec/mole of metal) ($\times 10^{+5}$)
NaC_{64}	7.5 ± 0.2
KC_8	3.3 ± 0.2
KC_n (4.5 wt% Fe)	5.8 ± 0.2
Fe/Al_2O_3 (14.9 wt% Fe)	117 ± 5

[a] Total initial pressure = 700 Torr.

via greased stopcocks to a conventional mercury-free high vacuum gas handling system. Initial pressures of H_2 and CO reactants were measured to ±0.1 Torr by a calibrated pressure transducer whose digital output was accurate to ±0.2% of reading. Furnace temperatures were regulated to ±0.5°C by a digital proportional band controller.

Reaction mixture components were separated by gas–solid chromatography, using a 3.2-mm-o.d. × 3.7-m stainless-steel column containing 80/100 mesh Porapak R and maintained at 80°C. Quantitative analyses were based on peak areas reported by a computing digital integrator from the output of a heated-filament thermal conductivity detector, following appropriate corrections for differing thermal responses of the various components.

Procedure. Sodium-graphite (NaC_{64}) and potassium-graphite (KC_8) samples were prepared *in situ* by transferring, under a dry nitrogen atmosphere, 0.5 g of graphite and an excess (0.5 g) of alkali metal into the catalytic reactor, evacuating for 16 hr at 25°C, and then heating the mixture in a static vacuum at 4°C/min to 300°C and maintaining at the latter temperature for 8 hr. A final dynamic evacuation for 16 hr at 300°C distilled excess alkali metal from the resulting intercalate and deposited it in an unheated region of the reactor. The same procedure was employed for preparation of iron-containing potassium-graphite samples (4.5 wt% Fe), except that the graphite used contained 12.0 wt% of previously intercalated iron(III) chloride. The latter intercalate was prepared by heating a stoichiometric mixture of graphite and anhydrous $FeCl_3$ in a closed, evacuated tube for 8 hr at 300°C. Previous studies, employing ^{57}Fe Mössbauer spectroscopy techniques, have demonstrated that treatment of $FeCl_3$-graphite with metallic potassium at 300°C effects reduction of Fe^{3+} to α-Fe (*20*). The structure of the resulting intercalated system is essentially that of KC_8, but with iron atoms (and KCl reduction by-product) dispersed randomly throughout the alkali metal sublattice.

All experiments were performed using a reaction temperature of 300°C and an initial H_2/CO reactant ratio of 4/1, at a total initial pressure of 700 Torr.

RESULTS AND DISCUSSION

Reaction Rates

Detailed kinetic studies and determinations of turnover frequencies for CO hydrogenation over the three graphite intercalation systems were not made. For comparison purposes, however, Table 1 summarizes the average initial reaction rates observed for three separate experiments with each of the freshly prepared materials. These initial rates declined rapidly with increasing extent of reaction, as discussed in a subsequent section. Also included in Table 1 is a representative initial rate observed for the iron/alumina comparison catalyst.

Reaction Selectivities

In each of the product distribution representations that follow, the mole fraction of each carbon-containing component has been corrected to account for the number of carbon atoms per molecule, and the results normalized to 100 moles of CO converted. Thus, the numerical difference

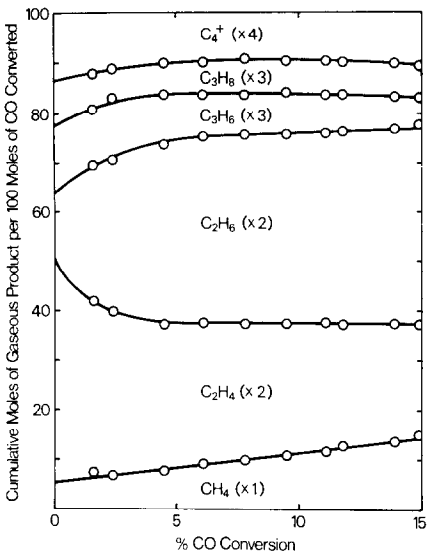

FIG. 1. Distribution of carbon-containing products over sodium-graphite (NaC_{64}) as a function of CO conversion at 300°C and an initial H_2/CO reactant ratio of 4/1 (total initial pressure = 700 Torr).

between an adjacent pair of plotted curves at a given conversion level corresponds to the percentage of all reacted CO that has been consumed in forming the indicated product.

Sodium-graphite. Figure 1 presents the cumulative distribution of all gaseous, carbon-containing products, as a function of total CO conversion, for a typical experiment employing a freshly prepared sample of NaC_{64}. (Due to an inherently marginal reproducibility in preparing the relatively ill-defined NaC_{64} composition, product distributions and initial reaction rates observed for this material were repeatable to only ±15%. The general features represented in Fig. 1 are, however, characteristic of all NaC_{64} samples studied.) Both paraffins and olefins appeared to be primary reaction products, with little indication of subsequent olefin hydrogenation. The amount of methane produced (5 to 15% of all CO reacted) was quite low, considering the relatively high reaction temperature (300°C) and H_2/CO reactant ratio (4/1) employed in these experiments. C_2 hydrocarbons constituted the major portion (60 to 65%) of carbon-containing products over the entire range of CO conversions investigated, but a substantial fraction (25 to 30%) of C_3^+ hydrocarbons was generated as well. Neither carbon dioxide nor oxygen-containing materials were observed with any of the NaC_{64} samples studied. The absence of CO_2 from the carbon-containing reaction products is significant and will be discussed in conjunction with the similar behavior of potassium-graphite described below.

Potassium-graphite. The propensity for C_2 hydrocarbon production exhibited by sodium-graphite was even more pronounced with potassium-graphite, as illustrated in Fig. 2 which contains a composite product distribution for three separate experiments, each employing a fresh KC_8 sample. Significantly, and unlike the behavior observed with NaC_{64}, however, unsaturated hydrocarbons were never observed among the gaseous reaction products over KC_8, even at low CO conversions. Ethane accounted for 80 to 85% of all reacted CO,

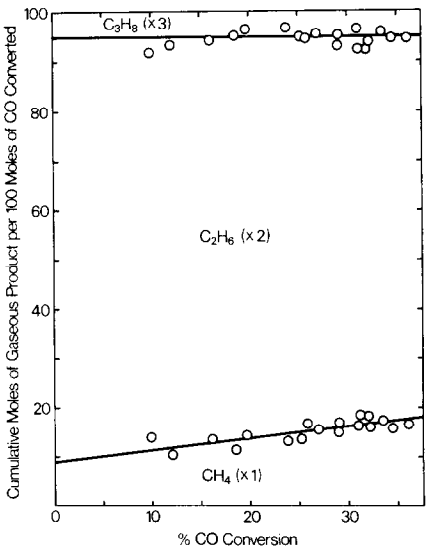

FIG. 2. Distribution of carbon-containing products over potassium-graphite (KC_8) as a function of CO conversion at 300°C and an initial H_2/CO reactant ratio of 4/1 (total initial pressure = 700 Torr).

up to 35% conversion, with methane (10 to 15%) and propane (~5%) constituting the remainder of the carbonaceous products. Neither oxygen-containing materials nor hydrocarbons higher than C_3 were observed. Although olefins are likely generated as the major or sole initial hydrocarbon products of CO conversion, their complete absence from the gaseous reaction products may be attributed to the marked hydrogenation capability of KC_8. Previous investigations have demonstrated that KC_8 is an effective hydrogenation catalyst for C_2–C_4 olefins at temperatures as low as 25°C (*15*). It is likely, therefore, that at 300°C and in the presence of excess H_2, initial generation of unsaturates over KC_8 during CO conversion would be followed by their immediate hydrogenation and consequent removal from the observed gaseous products. The olefin hydrogenation activity of sodium-graphite is evidently less pronounced than that of its potassium counterpart, although a gradual conversion of ethylene to ethane with increasing CO conversion is apparent in Fig. 1.

The high selectivities to C_2 hydrocarbons exhibited by both sodium- and potassium-graphites, particularly the latter, may be a result of the necessarily regular spacing of edge-type intercalated alkali metal atoms and, hence, the catalytically active sites that must be associated with them. The length of an adsorbed H_2C–CH_3 species (or

$$\downarrow$$

its two-carbon precursor), for example, from the point of attachment at or near an alkali metal atom/ion to the end of the methyl group is approximately 2.5 to 2.6 Å. Free rotation of such an entity in a plane perpendicular to those of the graphite layers would result in an excluded distance along the graphite *c* axis of 5.0 to 5.2 Å. Consequently, since the distance between adjacent layers of potassium atoms/ions in KC_8 is 5.4 Å (*7*), product chain growth beyond two carbons would be effectively hindered if each potassium species were catalytically active in the initially prepared state. The lower alkali metal population and less-ordered structure of NaC_{64}, on the other hand, results in considerably greater average distances between neighboring metal layers than is the case for KC_8, and would permit correspondingly longer carbon chain growth. The substantially larger fraction of C_3^+ hydrocarbons observed with sodium-graphite substrates may be consistent with this property.

The complete absence of carbon dioxide from the carbon-containing products obtained with both sodium- and potassium-graphites is significant, and reflects another important feature of these materials. Three potential sources of CO_2 normally exist during H_2/CO reactions, viz., from the disproportionation of CO reactant:

$$2\,CO \rightarrow C(s) + CO_2 \qquad (1)$$

as a byproduct of hydrocarbon formation:

$$2n\,CO + (n+1)\,H_2 \rightarrow C_nH_{2n+2} + n\,CO_2 \qquad (2a)$$

or

$$2n\,CO + n\,H_2 \rightarrow C_nH_{2n} + n\,CO_2 \qquad (2b)$$

and via the water–gas shift reaction, involving the water generated as a byproduct of CO hydrogenation:

$$CO + H_2O \rightleftharpoons CO_2 + H_2. \qquad (3)$$

The first two sources, particularly Reaction (1), normally make only minor contributions to the total amount of gaseous CO_2 observed during H_2/CO processes. The absence of carbon dioxide over both alkali metal-graphites could be attributed to the known capability of these materials to hydrogenate CO_2 to hydrocarbon products (*13*, *14*). It is more likely, however, that the immediate and irreversible removal of by-product water from the reaction mixture, via interaction with intercalated alkali metal, prevents the occurrence of Reaction (3) and thereby removes the principal source of gaseous CO_2 generation. This

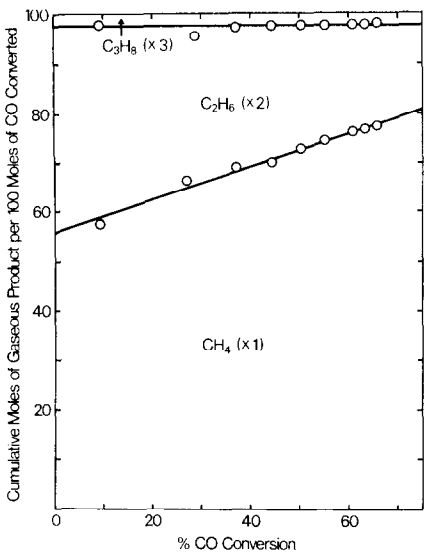

FIG. 3. Distribution of carbon-containing products over iron-containing potassium-graphite (4.5 wt% Fe) as a function of CO conversion at 300°C and an initial H_2/CO reactant ratio of 4/1 (total initial pressure = 700 Torr).

behavior leads to destruction of alkali metal centers and causes a gradual loss of catalytic activity (*vide infra*).

Iron-containing potassium-graphite. Introduction of 4.5 wt% of iron into a potassium-graphite intercalate had relatively little effect on the overall CO conversion activity (Table 1), but dramatically altered the product selectivity from that observed with pure KC_8, as shown in Fig. 3. Carbon dioxide and unsaturated hydrocarbons were again absent from the gaseous products, for the reasons discussed above, but methane now constituted the major product fraction, accounting for 60 to 80% of all CO reacted over the range of conversion investigated. The remainder of the carbon-containing product distribution was composed primarily of ethane which, however, decreased considerably with increasing reactor contact time due to apparent hydrogenolysis to methane. The amount of propane generated, as with KC_8 was relatively small and constant.

Although differing from that observed with pure KC_8, the selectivity of iron-containing potassium-graphite was equally uncharacteristic of the behavior exhibited by a "conventional," nongraphitic iron catalyst under the same reaction conditions. Figure 4 illustrates, for example, the product distribution observed for a typical experiment employing a hydrogen-reduced, alumina-supported iron catalyst (containing 14.9 wt% Fe). Apart from methane and the carbon dioxide generated via a shift reaction, the primary carbon-containing products observed in this case were olefins that underwent hydrogenation to their paraffinic counterparts with increasing contact time. In addition, and unlike the behavior displayed by iron-containing potassium-graphite, C_3^+ hydrocarbons accounted for as much as 25% of all CO reacted at >10% conversion, with little evidence for subsequent hydrocarbon hydrogenolysis.

The reason for the markedly greater selectivity to methane, and correspondingly decreased generation of C_2 hydrocarbons, exhibited by iron-containing potassium-

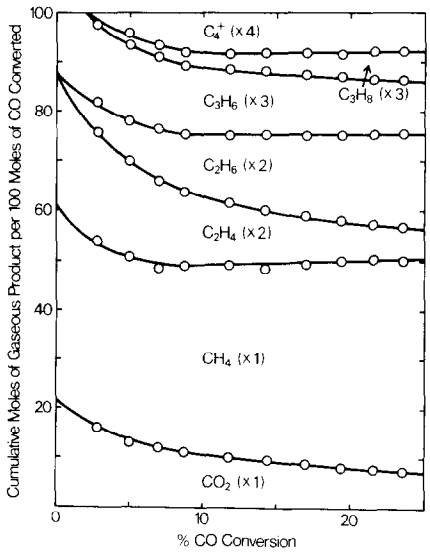

FIG. 4. Distribution of carbon-containing products over Fe/Al_2O_3 (14.9 wt% Fe) as a function of CO conversion at 300°C and an initial H_2/CO reactant ratio of 4/1 (total initial pressure = 700 Torr).

graphite in comparison to that of KC_8 is unclear, but may be due to an anomalous effect of a potassium–iron bimetallic system. In a single experiment, for example, when the Fe_2O_3/Al_2O_3 precursor of the supported iron catalyst described above was reduced with metallic potassium at 300°C (with subsequent removal of excess alkali metal by distillation), rather than with hydrogen, the sole carbon-containing product observed at a reaction temperature of 300°C was methane. Alternatively, the randomly dispersed iron atoms may both partially destroy the previously described spacing pattern of edge-type intercalated potassium species as well as serving as independent catalytic sites with a high selectivity to methane. Both features could make carbon chain growth beyond a single atom a less frequently occurring event than is the case for pure KC_8.

Catalyst Deactivation

The deactivation and CO adsorption behaviors of all three graphite intercalates were very similar, and will be discussed in detail for the case of KC_8, for which the largest amount of data is available. Freshly prepared KC_8 possessed a marked capacity for CO adsorption at 300°C. In a separate experiment, for example, exposure of KC_8 to excess CO for 30 min at 300°C prior to admission of the normal H_2/CO reaction mixture resulted in a complete absence of subsequent hydrogenation activity, presumably due to site saturation by adsorbed CO and consequent prevention of H_2 adsorption.

Figure 5 contains the results obtained for one of three comparable series of four consecutive experiments, employing a single sample of fresh KC_8, in which overnight evacuation at reaction temperature (300°C) followed the last plotted time in each run. The open points in each case represent the percentage conversion, based on total generated amounts of gaseous carbon-containing products, of all CO admitted into the reactor, while the solid points depict the percentage of unreacted CO remaining in the gas phase (i.e., unadsorbed), as determined by carbon mass balance calculations. Unreacted CO was rapidly adsorbed by the fresh KC_8 sample, as shown by the solid points for Run 1, and completely disappeared from the gas phase after approximately 60 min of exposure. Surface saturation by adsorbed CO was evidently incomplete, however, since hydrocarbon products continued to be generated even after complete removal of gaseous CO,

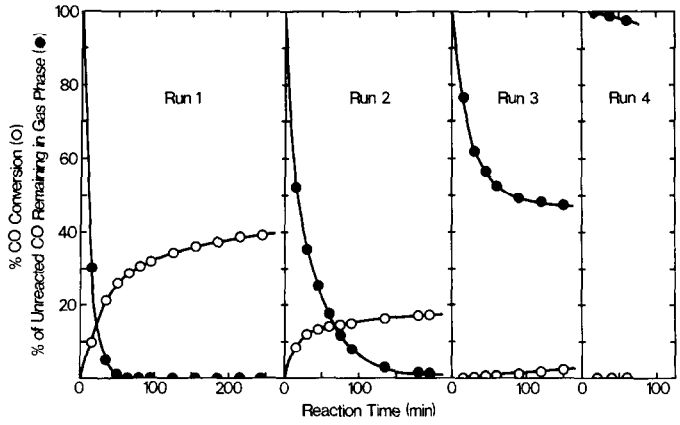

FIG. 5. Loss of CO adsorption capacity and hydrogenation activity during four consecutive runs over a single sample of KC_8 at 300°C and an initial H_2/CO reactant ratio in each case of 4/1 (total initial pressure = 700 Torr).

but only until ~40% of the originally admitted CO had reacted, after which product formation virtually ceased. Evacuation for 16 hr at 300°C partially restored hydrogenation activity (Run 2), but both the rate and extent of CO adsorption were lower than those observed for the fresh sample, and only 20% of the CO was converted to hydrocarbon products in this case before conversion halted. Since excess H_2 was still present in both experiments when product formation ceased, these results suggest that at least two forms of chemisorbed CO exist on KC_8 at 300°C, viz., a "reactive" species, capable of undergoing subsequent hydrogenation, and a strongly held but unreactive form that is resistant to interaction with gaseous or adsorbed H_2. This postulate is supported by the results obtained for the third experiment of the series, in which the sample still displayed considerable CO adsorption capacity (for the apparently unreactive variety), but little remaining activity for CO hydrogenation. By the fourth consecutive run, all catalytic activity and virtually all CO adsorption capacity had irrecoverably disappeared; further evacuation at 300°C or treatment with excess H_2 at the same temperature failed ro restore either hydrogenation or CO adsorption behavior.

The irreversible loss of catalytic behavior exhibited by potassium-graphite is due to permanent destruction of intercalated alkali metal atoms/ions (and, hence, the catalytically active sites associated with them) via interaction with the water molecules that are inevitably produced during CO hydrogenation. (Gaseous water was never observed in any of these experiments, regardless of the extent of CO conversion):

$$n\,CO + (2n + 1)\,H_2 \rightarrow C_nH_{2n+2} + n\,H_2O \quad (4)$$

$$K + H_2O \rightarrow KOH + \tfrac{1}{2}H_2. \quad (5)$$

It is this immediate and continuous removal of by-product water that prevents the occurrence of a water–gas shift process (Reaction 3), and is primarily responsible for the observed absence of carbon dioxide from the gaseous reaction products over alkali metal-graphite substrates. The original copper–bronze color of the freshly prepared KC_8 had become grayish-white following deactivation, due to the KOH generated by Reaction (5).

Total loss of hydrogenation activity during the series of experiments depicted in Fig. 5 occurred after a cumulative CO conversion for all four runs of approximately one CO molecule per three potassium atoms/ions in the originally prepared KC_8. Additional qualitative tests confirmed the presence of considerable unoxidized metallic potassium in the completely deactivated catalyst following its removal from the reactor. Assuming that the conversion of each CO molecule is accompanied by the formation of a water molecule that destroys a catalytic site, the apparent inacessibility of two-thirds of the sites associated with potassium species indicates that adsorption and subsequent hydrogenation of CO occurs primarily along exposed edges of the layered crystallites, and that interlayer penetration by CO reactant is minimal. This behavior is consistent with the relative dimensions of both molecular CO and the KC_8 lattice, shown schematically in Fig. 6 for a single graphitic

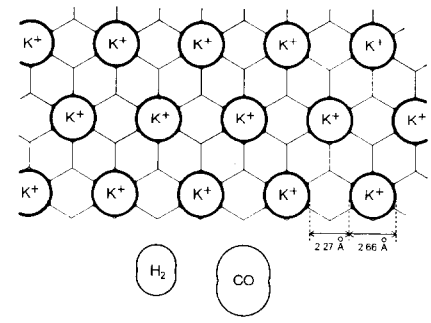

FIG. 6. Comparison of relative dimensions of molecular H_2 and CO with those of KC_8 lattice, assuming total ionization of intercalated potassium atoms.

layer. The situation depicted assumes total ionization of intercalated potassium atoms to K^+ species; for the more realistic case of only partial electron transfer, the average intermetallic distance would be even less than the value of 2.27 Å noted in Fig. 6. Based on this comparison, it is clear that penetration of molecular CO beyond edge-located potassium atoms/ions is unlikely. On the basis of adsorption studies at −196°C, Tamaru has previously suggested that interlayer penetration of the KC_8 lattice by molecular N_2 (virtually identical in size to CO) and even by H_2 does not occur due to space limitations (*21*).

Results analogous to those shown in Fig. 5 were obtained for both sodium-graphite and for iron-containing potassium-graphite samples. The behaviors of these materials differed only slightly from that of KC_8 with respect to the extents and rates of CO adsorption and the cumulative number of CO molecules converted per alkali metal entity at total deactivation. Reproducibility of the data for NaC_{64} in the latter regard was marginal, however, due to the nonstoichiometric nature of this material. It was significant that, in the case of the iron-containing potassium-graphite samples, no residual hydrogenation activity that could be ascribed to the transition metal component remained following complete destruction of edge-type potassium species, and total deactivation occurred at a cumulative CO conversion level that was virtually identical to that observed with unmodified KC_8. This behavior may be due to the blockage of potentially active iron sites by the KOH generated in Reaction (5) during potassium destruction.

CONCLUSIONS

Adsorption and subsequent hydrogenation of carbon monoxide on "sites" resulting from the charge–transfer process inherent in alkali metal-graphite intercalates may be viewed as a catalytic phenomenon. On a macroscopic basis, however, the reaction is noncatalytic and is, in fact, only partially stoichiometric, due to the lack of interplaner penetration by CO and to the unavoidable destruction of alkali metal species by the water molecules that are inevitably generated during CO conversion. It is likely, we feel, that the CO hydrogenation behaviors reported previously for several transition metal-containing potassium-graphites (*12*) are in every case those of slightly modified KC_8, and are not reflective of the activities of potassium-reduced intercalated metal atoms.

ACKNOWLEDGMENTS

The authors gratefully acknowledge financial support of this research by the U. S. Department of Energy under Contract No. E(49-18)-2467, and by the Texas A & M Center for Energy and Mineral Resources.

REFERENCES

1. Croft, R. C., *Aust. J. Chem.* **9**, 184 (1956).
2. Henning, G. R., *Progr. Inorg. Chem.* **1**, 125 (1959).
3. Croft, R. C., *Quart. Rev.* **14**, 1 (1960).
4. Novikov, Yu. N., and Vol'pin, M. E., *Russ. Chem. Rev.* **40**, 733 (1971).
5. Ebert, L. B., *Ann. Rev. Mater. Sci.* **6**, 181 (1976).
6. Nixon, D. E., and Parry, G. S., *Brit. J. Appl. Phys. (J. Phys. D)*, Ser. 2 **1**, 291 (1968).
7. Tamaru, K., and Ichikawa, M., "Catalysis by Electron Donor–Acceptor Complexes." Wiley, New York, 1975.
8. Robert, M. C., Oberlin, M., and Mering, J., "Chemistry and Physics of Carbon" (P. L. Walker and P. A. Thrower, Eds.), Vol. 10, p. 141. Marcel Dekker, New York, 1973.
9. Delhaes, P., *Mater. Sci. Eng.* **31**, 225 (1977).
10. Boersma, M. A. M., *Catal. Rev.-Sci. Eng.* **10**, 243 (1974).
11. Ichikawa, M., Sudo, M., Soma, M., Onishi, T., and Tamaru, K., *J. Amer. Chem. Soc.* **91**, 1538 (1969).
12. Ichikawa, M., Naito, S., Kawase, K., and Tamaru, K., U. S. Patent No. 3,842,121 (1974).
13. Naito, S., Ogawa, O., Ichikawa, M., and Tamaru, K., *J. Chem. Soc. Chem. Commun.* 1266 (1972).
14. Ichikawa, M., Naito, S., Kondo, T., Kawase, K., and Tamaru, K., U. S. Patent No. 3,842,113 (1974).

15. Ichikawa, M., Soma, M., Onishi, T., and Tamaru, K., *J. Catal.* **9**, 418 (1968).

16. Ichikawa, M., Inoue, Y., and Tamaru, K., *J. Chem. Soc. Chem. Commun.* 928 (1972).

17. Ottmers, D. M., and Rase, H. F., *Ind. Eng. Chem. Fund.* **5**, 302 (1966).

18. Sudo, M., Ichikawa, M., Soma, M., Onishi, T., and Tamaru, K., *J. Phys. Chem.* **73**, 1174 (1969).

19. Ichikawa, M., Kondo, T., Kawase, K., Sudo, M., Onishi, T., and Tamaru, K., *J. Chem. Soc. Chem. Commun.* 176 (1972).

20. Tricker, M. J. Evans, E. L., Cadman, P., and Davies, N. C., *Carbon* **12**, 499 (1974).

21. Tamaru, K., *Amer. Sci.* **60**, 474 (1972).